RSC Advances

PAPER

View Article Online
View Journal | View Issue

Cite this: *RSC Adv.*, 2020, **10**, 44835

A new strategy for synthesizing silver doped mesoporous bioactive glass fibers and their bioactivity, antibacterial activity and drug loading performance

Xiang Qin, Rong Cao, Jingjing Zheng, Guojun Shi, Lijun Ji, * Aiping Zhu* and Hang Yao*

A new strategy for preparing mesoporous metal-doped bioactive glass fibers (MBGFs) was designed, which included electrospinning and sulfonating mesoporous PS fibers, precipitating metal ions and bioactive glass sol–gel precursor into the mesoporous polystyrene (PS) fibers and calcinations. Silver-doped mesoporous BGFs (Ag-MBGFs) with a uniform diameter of 1–2 μm and a specific surface area of 40.22 $m^2\ g^{-1}$ were prepared as an example and characterized by SEM, XRD, TG, ICP and FTIR. These Ag-MBGFs showed excellent bioactivity, antibacterial properties and drug loading and release performance due to their special mesoporous and fibrous structure. The concentration of *Staphylococcus aureus* decreased from 1×10^8 colony-forming units per mL (CFU mL^{-1}) to 2.5×10^6 CFU mL^{-1} in 2 h and then to 2×10^2 CFU mL^{-1} in 12 h when the concentration of the Ag-MBGFs reached 16 mg mL^{-1}. BGFs of different compositions and functions could be prepared by the same strategy in a mesoporous PS fiber template, which could enrich materials for constructing orthopedic implants.

Received 11th October 2020
Accepted 25th November 2020

DOI: 10.1039/d0ra08656h

rsc.li/rsc-advances

1. Introduction

In recent years, bioactive glass fibers (BGFs) have been considered attractive constructing blocks for preparing three dimensional tissue engineering scaffolds and orthopedic implants, because bioactive glass (BG) has been confirmed as a material possessing excellent bioactivity, bone inductivity and ability to promote angiogenesis.[1–3] A fibrous implant constructed from BGFs can be used to mimic the fibrous extracellular matrix and porous bone tissue.[4–7] Their high specific surface area is helpful for rapid ion release and protein absorption, which are very important for bone conduction.[8–10] In addition, BGFs can be used as fillers to reinforce dental resins or other polymer matrix,[11,12] and the efficacy of BG/PVB nanofibers for oral mucosal regeneration has been reported in recent.[13] BGFs have been prepared by a glass drawing method,[14] a laser spinning technology,[15] and an electrospinning method.[16] Electrospinning is the most popular method for preparing BGFs of nanoscale diameter. Mesoporous BGFs (MBGFs) are prepared by using nonionic surfactant as a pore-forming agent for electrospinning.[17–19]

Silver is considered a promising metal element to be incorporated with BGs to prepare BG implants and scaffolds for tissue engineering due to its excellent antibacterial property. It is confirmed that an Ag_2O-doped BG possesses broad spectrum antibactericidal activity.[20] Monodispersed BG microspheres modified with silver nitrate are synthesized by a modified Stöber method, and show antibacterial capability.[21] The antibacterial capability of an Ag_2O-doped BG is related to the doping amount, and combining 10 mol% of Ag_2O with BGs does not decrease the biocompatibility of BGs.[22] Porous structure is helpful for silver ion release and high inhibition performance to bacteria.[23] Mesoporous BGs incorporated with silver present enhanced antibacterial property.[24] Silver-doped BG is a promising dental material because dental implants are constantly exposed to bacteria. Silver-doped BG/mesoporous silica composite particles show excellent antibacterial performance and high rate of dentinal tubule occlusion.[25] A BG combined with silver nanoparticles indicates bactericidal effect against *Enterococcus faecalis* which exists in root canal system.[26] These reports suggest that silver-doped BGs are potential building blocks for preparing orthopedic implants. Fibers prepared by silver-doped BGs can be used to engineer fibrous implants with antibacterial property. PCL composite fibers combined with silver-doped mesoporous BGs have been successfully prepared and show great potential in tissue engineering.[27] However, to the authors' knowledge, silver-doped mesoporous bioactive glass fibers (Ag-MBGFs) have not been reported due to the lack of suitable preparation method.

The purpose of this work is to explore a strategy for preparing metal-doped bioactive glass fibers by trying to template

College of Chemistry and Chemical Engineering, Yangzhou University, Yangzhou, 225002, China. E-mail: yaohang@yzu.edu.cn

synthesize Ag-MBGFs and investigate their properties. Mesoporous polystyrene (PS) fibers were prepared by electrospinning and used as a template for replicating Ag-MBGFs. We suppose that these Ag-MBGFs should have excellent bioactivity, antibacterial performance and ideal drug loading and release capability.

2. Experimental

2.1. Preparation of Ag-MBGFs

All the reagents were purchased from Aladdin Industrial Corporation and used as received. 4 g of polystyrene (PS, M_w = 110 000) synthesized in our laboratory and 0.1 g of benzyl triethyl ammonium chloride were dissolved in 16 g of DMF and stirred at room temperature for 2 h. The solution was electrospun at 23 °C with a voltage of 15 kV to prepare mesoporous PS fibers. The PS fibers were immersed in 98% concentrated sulfuric acid for sulfonation at 80 °C for 0.5 h, and the obtained sulfonated polystyrene (SPS) fibers were washed with water for three times and then ethanol for three times. 8 g of $Ca(NO_3)_2 \cdot 4H_2O$ was dissolved in 100 mL of ethanol to make a solution in which the SPS fibers were immersed for 24 h. The SPS fibers soaked with $Ca(NO_3)_2$ were immerse in 100 mL of saturated silver nitrate ethanol solution for 6 h and 20 mL of 30% (v/v) TEOS ethanol solution for 24 h in turn. The samples were taken out and dried at 80 °C, and extracted with tetrahydrofuran at 80 °C for 3 h. After being dried, the fibers were calcined in a muffle furnace at 600 °C to remove the organic component. Finally, Ag-MBGFs were obtained.

2.2. Characterization of materials

The morphology of the samples was investigated by a scanning electron microscopy (SEM, Hitachi, S4800-11). The phase composition of the sample was examined by an X-ray diffractometry (XRD). The specific surface area and pore distribution of the samples were measured by the Brunauer–Emmett–Teller (BET) and the Barret–Joyner–Halenda (BJH) method (Bei Shi, De3H-2000PS2). The functional groups and molecular structures of the samples were analyzed by a Fourier transform infrared spectroscopy (FTIR, Bruker, Tensor27). The sample was dried for 24 h in an oven at 60 °C and then characterized by thermal gravity analysis (TGA, PerkinElmer).

2.3. *In vitro* bioactivity test

The evaluation of *in vitro* bioactivity was performed by observing hydroxyapatite (HA) formed on the samples which were immersed in a simulated body fluid (SBF) solution in a concentration of 0.001 mg mL^{-1} and placed in a shaker (37 °C, 170 rpm). SBF (NaCl, $NaHCO_3$, KCl, $K_2HPO_4 \cdot 3H_2O$, $MgCl_2 \cdot 6H_2O$, $CaCl_2$, Na_2SO_4, Tris(hydroxymethyl)aminomethane and HCl) was prepared as explained by Kokubo *et al.*[28] Samples taken on 3 d, 7 d, and 14 d were separated from the SBF solution by centrifugation, washed with deionized water and dried at 60 °C. Finally, the degraded samples were characterized by SEM, XRD and FTIR. The concentration of silver, silicon, calcium and phosphorus in SBF solution was determined by an inductively coupled plasma spectrometer (ICP, Optima 7300 DV).

2.4. Evaluation of bacteriostatic activity

The bacteriostatic activity was evaluated according to the national food safety standard of China (GB 4789.10-2016) and the report.[8,9] In order to determine the inhibition effect on the growth of *Staphylococcus aureus*, different quantitative Ag-MBGFs were added into a mixture combined with 0.2 mL of *Staphylococcus aureus* (2×10^7 CFU mL^{-1}) and 4.8 mL of PBS medium, and then placed in an incubator at 37 °C for 12 h. After diluting the obtained bacterial suspensions to 10^{-1}, 10^{-2}, 10^{-3}, 10^{-4}, 10^{-5}, 10^{-6}, 10^{-7}, 10^{-8}, 10^{-9}, 10^{-10}, 10^{-11}, 10^{-12}, 10^{-13}, 10^{-14}, 10^{-15}, 50 μL of the diluents were distributed on the blood agar medium at 37 °C for 24 h to evaluate the inhibition of Ag-MBGFs on *Staphylococcus aureus*. The number of colonies on the plate was translated into the number of viable cells. Finally, a spectrophotometer was used to measure the photometric values of samples with different concentrations after 12 h of inhibition. The mean value and standard deviation were obtained by testing five species for each condition.

2.5. The ibuprofen drug loading and release

100 mg of Ag-MBGFs was soaked in 2 mL of ibuprofen/hexane solution (60 mg mL^{-1}) for 12 h, and then removed from the ibuprofen/hexane solution and dried at 60 °C. The Ag-MBGFs loaded with ibuprofen was immersed in 100 mL of SBF solution, releasing ibuprofen in a shaking table at 37 °C. 2 mL of SBF solution was taken out at a certain interval and replaced by the same amount of fresh SBF. The concentration of ibuprofen was test at 262 nm by a UV-visible photometer.

2.6. *In vitro* cytotoxicity

The material was cleaned twice with sterile water, and then sterilized in an oven at 120 °C for 1 h. The Ag-MBGFs were immersed in culture solution at concentrations of 2 mg mL^{-1} and 200 mg mL^{-1} for 24 h. And then the culture solutions were used to culture human skin fibroblast cells (HSF) in 24-well plates. WST and live and dead staining were performed to measure the metabolic activity of cells after culturing for 24 h. Three groups of normal cultured cells were set as control groups. The experimental groups were repeated three times.

2.7. Statistical analysis

Statistical analysis was performed using one-way analysis of variance (ANOVA) with *post hoc* test. Results are expressed as mean ± standard error of the mean of triplicate determinations. Differences were considered statistically significant at $p < 0.05$.

3. Results and discussions

3.1. Template synthesis and characterization of Ag-MBGFs

As shown in Fig. 1a, the mesoporous PS fiber templates prepared by an electrospinning method were about 1 μm in diameter.[29] These fibers were full of interconnected pores which

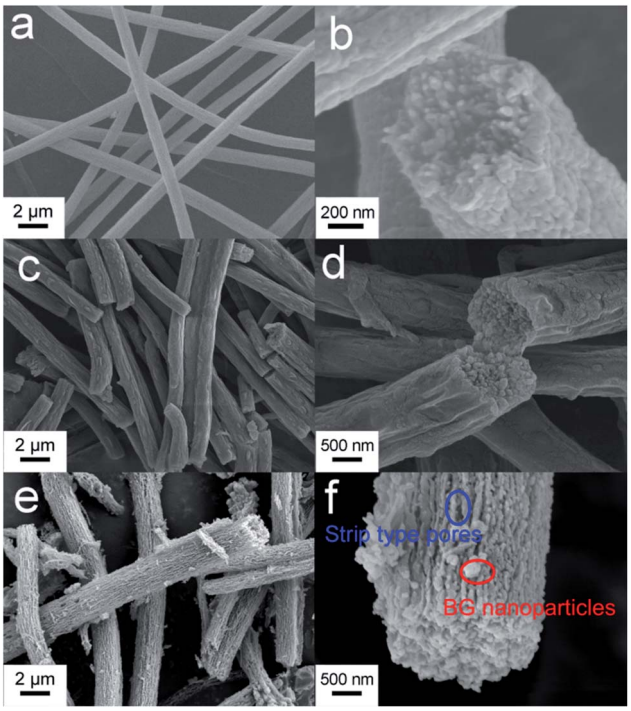

Fig. 1 (a) The PS fibers prepared with a PS electrospun solution of 20 wt%; (b) the magnified image of PS fibers showed a mesoporous structure; (c) the PS fibers sulfonated by sulfuric acid showed SPS surface; (d) the morphology of the PS fibers changed due to the formation of SPS layer; (e) the Ag-MBGFs were obtained by co-pyrolysis; (f) an image of the cross section showed the mesoporous structure throughout the Ag-MBGFs.

could be seen by observing the cross section of the fibers (Fig. 1b). SPS layers were formed on the surface of the fibers because of the reaction of sulfuric acid with polystyrene.[30,31] These SPS layers expanded and blocked part of the mesoporous structure (Fig. 1c and d). It has been confirmed that an acidic hydrogel layer on fibers or particles can absorb titania or silica precursor and catalyze the sol–gel reaction of them to happen in the layer.[32] In this case, the SPS layer could absorb silver and calcium ions and form sulfonates in it firstly, and then silica was catalyzed to form in it. Ag-MBGFs were obtained after pyrolyzing all organic composite, silver nitrate and calcium nitrate. An SEM image showed that the Ag-MBGFs remained the diameter of the SPS fiber templates (Fig. 1e). A magnified image showed that every Ag-MBGF was a bundle of thinner nanofibers which were composed of many BG nanoparticles, leaving many concentric strip voids between the nanofibers (Fig. 1f). These strip voids could be formed when the SPS fiber templates were removed. This special fibrous structure composed of concentric strip voids and connected nanoparticles effectively improved the specific surface area of the Ag-MBGFs. Fig. 2 showed the nitrogen adsorption/desorption isotherms and corresponding pore size distribution of the Ag-MBGFs. Most of pores distributed in two ranges. The pore distribution in the range of 3–10 nm could be assigned to those mesopores among the BG nanoparticles formed by a sol–gel process,[4,5] and those in the range of 20–40 nm could be assigned to the strip type voids

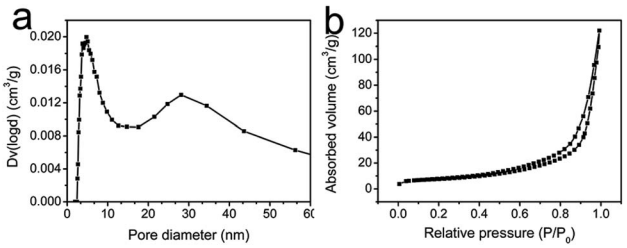

Fig. 2 (a) The pore size distribution of Ag-MBGFs; (b) the N_2 adsorption/desorption isotherm of Ag-MBGFs.

between the nanofibers (Fig. 2a). The specific surface area of the Ag-PBGFs was 40.22 m^2 g^{-1}. The adsorption/desorption isotherm was the type III curve of H3 lagging ring (Fig. 2b), without saturated adsorption platform, which was generally attributed to a thermodynamics or network structure or a combination of the two.[33] The mesoporous structure formed inside the Ag-MBGFs was conducive to the adsorption of small molecules. EDS characterization confirmed that silver ions were incorporated into BGFs (Table 1). A mapping image of Ag-MBGFs showed that Ca, Si, O, Ag signals were distributed evenly in the fiber, confirming that Ag_2O were incorporated uniformly in BGFs (Fig. 3).

3.2. *In vitro* bioactivity

Fig. 4 showed the surface morphology of Ag-MBGFs degraded in SBF for 3 d, 7 d and 14 d. Many lamellar HA crystals formed on Ag-MBGFs after degradation for 3 d (Fig. 4a). The amount of lamellar HA crystal increased and covered Ag-MBGFs completely after degradation for 14 d (Fig. 4b–d). ICP result of the SBF solution confirmed that silver and silicon emerged in 3 d and their concentration in SBF kept on increasing due to the ion release of Ag-MBGFs (Fig. 5). Meanwhile, the release profile of silver and silicon were synchronized completely (Fig. 5a and b), implying that silver could release continuously following the degradation of an implant made of the Ag-MBGFs, which was helpful for a long-term bactericidal effect. The concentrations of calcium increased in 3 d, and decreased subsequently, suggesting that the release of calcium by Ag-MBGFs had the superiority in the first 3 d and the precipitation of HA took the superiority subsequently. The concentration of phosphorus from the SBF decreased to be lower than original SBF (Fig. 5d), suggesting that phosphorus was precipitated following the formation of HA. The ICP result was consistent with that of SEM observation.

The FTIR and XRD spectra of Ag-MBGFs immersed in SBF solution for 3 d, 7 d and 14 d also confirmed the result of SEM (Fig. 6). The peak at 471 cm^{-1} was attributed to the Si–O bending vibration of the Ag-MBGFs; the peak at 795 cm^{-1} was

Table 1 The composition of the Ag-MBGFs (not including oxygen)

Element names	Si	Ca	Ag	Si/Ca
Atomic percent (%)	87.48	10.68	1.84	8.20

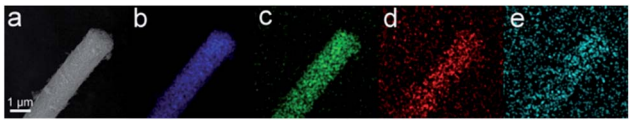

Fig. 3 The mapping image of Ag-MBGFs. (a) The fiber of Ag-PBGFs; (b) Si; (c) O; (d) Ca; (e) Ag.

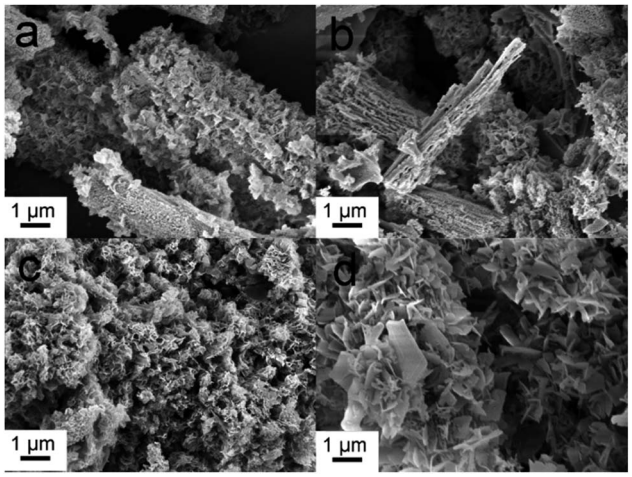

Fig. 4 The SEM images of Ag-MBGFs after degradation in SBF for: (a) 3 d; (b) 7 d and (c) 14 d; and (d) a magnified image of HA covered on the Ag-MBGFs.

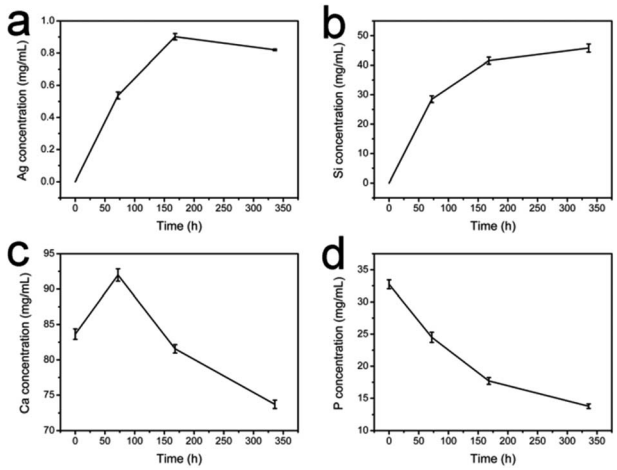

Fig. 5 The ICP result of SBF with the Ag-PBGFs degrading in it for 3 d, 7 d and 14 d: (a) silver; (b) silicon; (c) calcium and (d) phosphorus.

attributed to the Si–O symmetric stretching vibration; and the peak at 1081 cm^{-1} was attributed to the Si–O asymmetric stretching vibration. Compared with the original Ag-MBGFs, a new absorption peak occurred near 600 cm^{-1} in all samples after degradation for 3 d, corresponding to the characteristic peak of PO_4^{3-} in HA, and the peak intensity increased gradually with time, while the P–O bending vibration peak at 958 cm^{-1} also emerged and increased gradually,[34,35] suggesting that HA was formed gradually on the surface of Ag-MBGFs. The XRD spectra of Ag-MBGFs soaked in SBF showed there was no

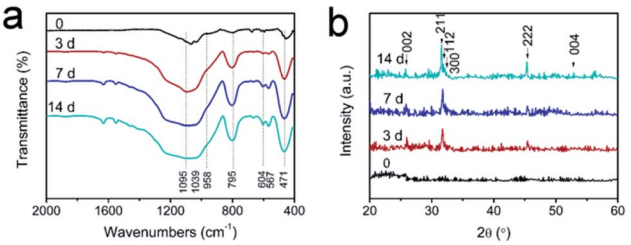

Fig. 6 The FTIR and XRD spectra of Ag-MBGFs after degradation in SBF for 3 d, 7 d and 14 d.

diffraction peaks of silver in the sample. The reason could be that the concentration of silver in the sample was very low and it did not form enough crystals. The dispersion peak of amorphous silica appeared at about 22°, and the characteristic peak of HA appeared at 45.3° and 26° after degradation for 3 d.[36] In 14 d, more characteristic peaks of HA appeared at $2\theta = 26°$, 32–35°, 53°, *etc.*, indicating that more HA was grown on Ag-MBGFs, which was consistent with the FTIR spectra.

3.3. *In vitro* antibacterial activity

As shown in Fig. 7a, the number of *Staphylococcus aureus* decreased significantly with the increase of Ag-MBGFs concentration in 12 h, showing excellent antibacterial effect. When 16 mg mL^{-1} of Ag-MBGFs was added, a certain bacteriostatic effect was observed (Fig. 7b). In 1 h, it not only showed a bacteriostatic effect, but also showed a certain bactericidal performance. The rapid bactericidal effect on *Staphylococcus aureus* could be attributed to the promotion of the mesoporous structure on the quick release of silver ions.[8,37]

3.4. Drug loading and release capacity

The special fibrous structure of the Ag-MBGFs is suitable for drug loading and release, because there were two sizes of mesopores, well interconnected strip type voids and mesopores in the nanofibers, in the Ag-MBGFs, as confirmed by the BJH result (Fig. 2a). The TG analysis of Ag-MBGFs-ibuprofen showed that the weight ratio of ibuprofen loaded in the Ag-MBGFs following the proposal of this work was 17.98% (Fig. 8a). Meanwhile, the infrared spectroscopy showed that the material was successfully loaded with ibuprofen (Fig. 8b). The ibuprofen

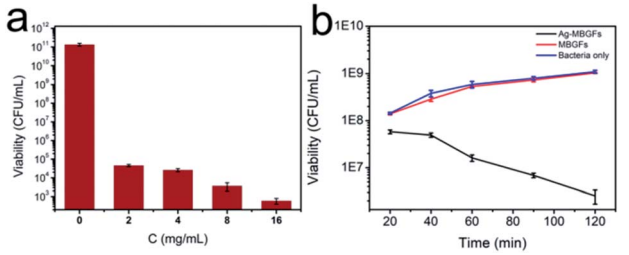

Fig. 7 (a) The effects of variable concentrations of Ag-PBGFs on growth and viability of the *Staphylococcus aureus* (12 h exposure); (b) the antibacterial effect of Ag-PBGFs on *Staphylococcus aureus* in different exposure time (16 mg mL^{-1}).

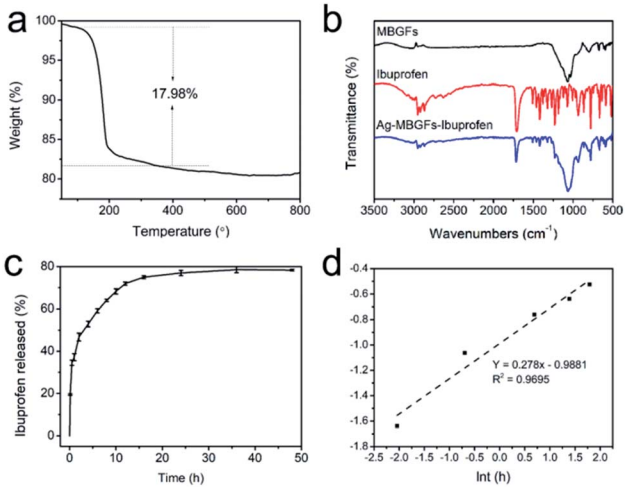

Fig. 8 (a) The TG curve showed the weight ratio of ibuprofen loaded in the Ag-MBGFs; (b) the FTIR spectra of ibuprofen loaded Ag-MBGFs; (c) the drug release profile of ibuprofen in the Ag-MBGFs; (d) the ln(fractional release of ibuprofen) plotted as a function of ln(time) using the data below 6 h.

in Ag-MBGFs could consist of two parts. One part was filled in the bigger strip type voids and attached on the surface of the nanofibers composed of the Ag-MBGFs, and the other part was filled in the smaller mesopores among the nanoparticles. These two parts of drug released in two steps. As could be seen from Fig. 8c, ibuprofen released about 34% in about 0.5 h, which was due to the rapid release of ibuprofen in the bigger strip type voids and on the surface of nanofibers. After that, ibuprofen in the smaller mesopores diffused slowly into the strip type voids, and then released into SBF solution, which made the final release amount of ibuprofen to be about 78% in 24 h. The release mechanism of ibuprofen was confirmed by fitting the *in vitro* data into the Korsmeyer–Peppas model. Only data below 6 h was used for fitting because the Korsmeyer–Peppas model was applicable for a fraction release (F) below 0.6.[38] The average value of n was equal to 0.278 (Fig. 8d), suggesting that the ibuprofen release conformed to Fick diffusion release mechanism. The diffusion of ibuprofen among the strip type voids could be determined to the release behavior.

3.5. *In vitro* cytotoxicity

Fig. 9 and 10 showed the metabolism of fibroblasts cultured at two different concentrations of MBGFs and Ag-MBGFs. The

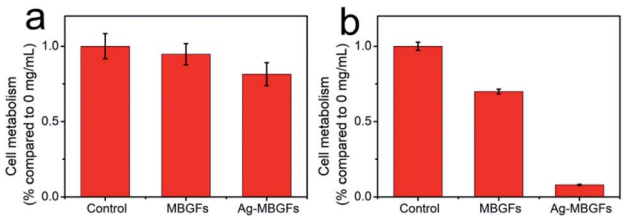

Fig. 9 Toxicity assay of the Ag-MBGFs to HSF cells in 24 h. (a) 2 mg mL; (b) 200 mg mL^{-1}.

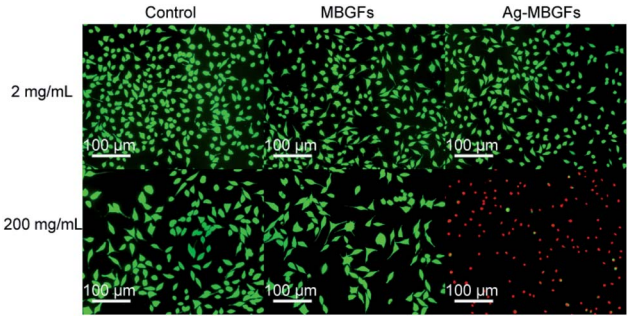

Fig. 10 HSF cells were stained alive and dead at 24 h.

culture solution immersed with 2 mg mL^{-1} of Ag-MBGFs, which showed significant antibacterial activity (Fig. 7a), slightly repressed the proliferation of HSF cells. The cell metabolism was significantly reduced when a culture solution immersed with Ag-MBGFs of high concentration (200 mg mL^{-1}) was used for culturing cells. The result was in consistent with a report,[39] and suggested that the concentration of Ag-MBGFs should not be high when they were used *in vivo*.

4. Conclusion

In conclusion, we designed a strategy for preparing Ag-MBGFs by using mesoporous PS fibers as templates. The Ag-MBGFs showed excellent bioactivity and drug loading and release performance due to a special fibrous and mesoporous structure with two sizes of mesopores. At the same time, the Ag-MBGFs were confirmed outstanding antibacterial effect on *Staphylococcus aureus*, because the mesoporous fibrous structure promoted the rapid release of silver from the material to the solution. It can be expected that the Ag-MBGFs could be a promising building block for constructing tissue engineering scaffolds and orthopedic implants with a fibrous structure and antibacterial property. This work enlightens us that mesoporous PS fibers are perfect templates for synthesizing BGFs containing large amount of charges, and more metal-doped BGFs can be prepared by the same template synthesis strategy.

Conflicts of interest

There are no conflicts to declare.

Acknowledgements

This work was supported by the National Natural Science Foundation of China (No. 51273171), the Natural Science Foundation of Jiangsu Province (No. BK20131226) and a project funded by the Priority Academic Program Development of Jiangsu Higher Education Institutions.

References

1 L. L. Hench and I. Thompson, *J. R. Soc., Interface*, 2010, 7, S379–S391.

2 D. Arcos and M. Vallet-Regi, *Acta Biomater.*, 2010, **6**, 2874–2888.
3 A. A. Gorustovich, J. A. Roether and A. R. Boccaccini, *Tissue Eng., Part B*, 2010, **16**, 199–207.
4 L. Ji, Y. Si, A. Li, W. Wang, D. Qiu and A. Zhu, *Front. Chem. Sci. Eng.*, 2012, **6**, 470–483.
5 J. R. Jones, S. Lin, S. Yue, P. D. Lee, J. V. Hanna, M. E. Smith and R. J. Newport, *Proc. Inst. Mech. Eng., Part H*, 2010, **224**, 1373–1387.
6 H. W. Kim, H. E. Kim and J. C. Knowles, *Adv. Funct. Mater.*, 2006, **16**, 1529–1535.
7 S. Chen, S. K. Boda, S. K. Batra, X. Li and J. Xie, *Adv. Healthcare Mater.*, 2017, 1701024.
8 Z. Ma, G. Dong, C. Lv and J. Qiu, *Mater. Lett.*, 2012, **88**, 136–139.
9 G. Novajra, N. G. Boetti, J. Lousteau, S. Fiorilli, D. Milanese and C. Vitale-Brovarone, *Mater. Sci. Eng., C*, 2016, **67**, 570–580.
10 A. El-Fiqi, J. H. Kim and H. W. Kim, *ACS Appl. Mater. Interfaces*, 2015, **7**, 1140–1152.
11 M. R. Syed, N. Z. Bano, S. Ghafoor, H. Khalid, S. Zahid, U. Siddiqui, A. S. Hakeem, A. Asif, M. Kaleem and A. S. Khan, *Ceram. Int.*, 2020, **46**, 21623–21631.
12 A. Mishra, P. Noppari, C. Boussard-Plédel, L. Petit and J. Massera, *Int. J. Appl. Glass Sci.*, 2020, **11**, 622–631.
13 N. Elshazly, A. Khalil, M. Saad, M. Patruno, J. Chakraborty and M. Marei, *Materials*, 2020, **13**, 2603.
14 E. A. A. Neel, I. Ahmed, J. J. Blaker, A. Bismarck, A. R. Boccaccini, M. P. Lewis, S. N. Nazhata and J. C. Knowlesa, *Acta Biomater.*, 2005, **1**, 553–563.
15 M. M. Echezarreta-López, T. D. Miguel, F. l. Quintero, J. Pou and M. Landín, *J. Biomater. Appl.*, 2017, **31**, 819–831.
16 A. M. Deliormanl, *Ceram. Int.*, 2016, **42**, 897–906.
17 Y. Hong, X. Chen, X. Jing, H. Fan, B. Guo, Z. Gu and X. Zhang, *Adv. Mater.*, 2010, **22**, 754–758.
18 C. Gao, Q. Gao, X. Bao, Y. Li, A. Teramoto and K. Abe, *J. Am. Ceram. Soc.*, 2011, **94**, 2841–2845.
19 J. Yi, G. Wei, X. Huang, L. Zhao, Q. Zhang and C. Yu, *J. Sol-Gel Sci. Technol.*, 2008, **45**, 115–119.
20 M. Bellantone, H. D. Williams and L. L. Hench, *Antimicrob. Agents Chemother.*, 2002, **46**, 1940–1945.
21 K. Dominika, Z. Kai, B. Elena, L. Yufang, L. Liliana and B. Aldo, *Materials*, 2016, **9**, 225.
22 A. Vulpoi, L. Baia, S. Simon and V. Simon, *Mater. Sci. Eng., C*, 2012, **32**, 178–183.
23 A. A. El-Rashidy, G. Waly, A. Gad, A. A. Hashem, P. Balasubramanian, S. Kaya, A. R. Boccaccini and I. Sami, *J. Non-Cryst. Solids*, 2018, **483**, 26–36.
24 K. Zheng, P. Balasubramanian, T. E. Paterson, R. Stein, S. MacNeil, S. Fiorilli, C. Vitale-Brovarone, J. Shepherd and A. R. Boccaccini, *Mater. Sci. Eng., C*, 2019, **103**, 109764.
25 J. H. Jung, D. H. Kim, K. H. Yoo, S. Y. Yoon, Y. Kim, M. K. Bae, J. Chung, C. C. Ko, Y. H. Kwon and Y. I. Kim, *Clin. Oral Investig.*, 2019, **23**, 253–266.
26 J. C. Kung, Y. J. Chen, Y. C. Chiang, C. L. Lee, Y. T. Yang-Wang, C. C. Hung and C. J. Shih, *J. Non-Cryst. Solids*, 2018, **502**, 62–70.
27 F. E. Ciraldo, L. Liverani, L. Gritsch, W. H. Goldmann and A. R. Boccaccini, *Materials*, 2018, **11**, 692.
28 T. Kokubo and H. Takadama, *Biomaterials*, 2006, **27**, 2907–2915.
29 C. L. Casper, J. S. Stephens, N. G. Tassi, D. B. Chase and J. F. Rabolt, *Macromolecules*, 2004, **37**, 573–578.
30 Z. Z. Yang, Z. W. Niu, Y. F. Lu, Z. B. Hu and C. C. Han, *Angew. Chem., Int. Ed.*, 2003, **42**, 1943–1945.
31 L. Ji, Y. Zhang, S. Miao, M. Gong and X. Liu, *Carbon*, 2017, **125**, 544–550.
32 L. Ji, X. Liu, T. Xu, M. Gong and S. Zhou, *J. Sol-Gel Sci. Technol.*, 2019, **93**, 380–390.
33 S. Huang, X. Kang, Z. Cheng, P. Ma, Y. Jia and J. Lin, *J. Colloid Interface Sci.*, 2012, **387**, 285–291.
34 S. Wang, *Microporous Mesoporous Mater.*, 2009, **117**, 1–9.
35 S. Cañaveral, D. Morales and A. F. Vargas, *Mater. Lett.*, 2019, **255**, 126575.
36 Y. Zhu and S. Kaskel, *Microporous Mesoporous Mater.*, 2009, **118**, 176–182.
37 F. Pishbin, V. MouriñO, J. B. Gilchrist, D. W. Mccomb, S. Kreppel, V. Salih, M. P. Ryan and A. R. Boccaccini, *Acta Biomater.*, 2013, **9**, 7469–7479.
38 Y. Zhu, J. Shi, Y. Li, H. Chen, W. Shen and X. Dong, *Microporous Mesoporous Mater.*, 2005, **85**, 75–81.
39 H. Wang, S. Zhao, X. Cui, Y. Pan, W. Huang, S. Ye, S. Luo, M. N. Rahaman, C. Zhang and D. Wang, *J. Mater. Res.*, 2015, **30**, 2722–2735.

